

See discussions, stats, and author profiles for this publication at: <https://www.researchgate.net/publication/253043462>

3D Lung Image Retrieval Using Localized Features

Article in *Proceedings of SPIE - The International Society for Optical Engineering* · October 2011

DOI: 10.1117/12.877943

CITATIONS

29

READS

309

4 authors:



Adrien Depeursinge

HES-SO Valais-Wallis

184 PUBLICATIONS 3,077 CITATIONS

[SEE PROFILE](#)



Tatjana Zrimec

UNSW Sydney

65 PUBLICATIONS 304 CITATIONS

[SEE PROFILE](#)



Sata Busayarat

UNSW Sydney

13 PUBLICATIONS 113 CITATIONS

[SEE PROFILE](#)



Henning Müller

HES-SO Valais-Wallis

838 PUBLICATIONS 15,023 CITATIONS

[SEE PROFILE](#)

Some of the authors of this publication are also working on these related projects:



Steerable Wavelet Machines (SWM) [View project](#)



ChaLearn Looking At People: First Impressions [View project](#)

3D Lung Image Retrieval Using Localized Features

Adrien Depeursinge^{a,b}, Tatjana Zrimec^{c,d}, Sata Busayarat^{d,e}, Henning Müller^{a,b}

^aUniversity of Applied Sciences Western Switzerland (HES-SO), Sierre, Switzerland;

^bUniversity and University Hospitals of Geneva, Medical Informatics, Geneva, Switzerland;

^cHealth Informatics, Faculty of Medicine, University of New South Wales, Sydney, Australia;

^dComputer Science and Engineering, University of New South Wales, Sydney, Australia;

^eMicrosoft Corporation, One Microsoft Way, Redmond, WA 98052-6399, USA;

ABSTRACT

The interpretation of high-resolution computed tomography (HRCT) images of the chest showing disorders of the lung tissue associated with interstitial lung diseases (ILDs) is time-consuming and requires experience. Whereas automatic detection and quantification of the lung tissue patterns showed promising results in several studies, its aid for the clinicians is limited to the challenge of image interpretation, letting the radiologists with the problem of the final histological diagnosis. Complementary to lung tissue categorization, providing visually similar cases using content-based image retrieval (CBIR) is in line with the clinical workflow of the radiologists.

In a preliminary study, a Euclidean distance based on volume percentages of five lung tissue types was used as inter-case distance for CBIR. The latter showed the feasibility of retrieving similar histological diagnoses of ILD based on visual content, although no localization information was used for CBIR. However, to retrieve and show similar images with pathology appearing at a particular lung position was not possible. In this work, a 3D localization system based on lung anatomy is used to localize low-level features used for CBIR. When compared to our previous study, the introduction of localization features allows improving early precision for some histological diagnoses, especially when the region of appearance of lung tissue disorders is important.

Keywords: Content-based medical image retrieval, 3D lung atlas, texture analysis, chest high-resolution CT, localized features, interstitial lung diseases.

1. INTRODUCTION

Interstitial lung diseases (ILD) group more than 150 disorders of the lung tissue from various causes leading to breathing dysfunction. Many of them are rare and present unspecific symptoms such as altered pulmonary functions and cough. Diagnosing ILDs is a difficult task for non-specialists and is based on observations of clinical, physiologic, pathologic manifestations as well as radiologic findings.¹ The latter occupy an important role as they allow assessing the appearance of the lung parenchyma, which is often representative of a particular histological diagnostic of ILDs.² The most employed imaging technique is the chest X-ray due to its low cost and limited radiation dose. However, it allows limited diagnosing specificity for ILDs as the lung tissue is superimposed with ribs and other organs. When the clinical and physiological presentations arouse suspicions towards an ILD, the HRCT imaging protocol is favored as it enables accurate visual assessment of the lung parenchyma by providing three-dimensional images at a sub-millimetric resolution in axial slices. The interpretation of high-resolution computed tomography (HRCT) images of the chest showing disorders of the lung tissue associated with ILDs is time-consuming and requires experience as the various diagnoses of ILDs are can be differentiated only by subtle changes in the lung parenchyma, with characteristic distribution within the lung anatomy.

Image-based computerized diagnosis aid tools were proposed to assist the radiologists in the HRCT interpretation tasks. Automatic detection and quantification of the lung tissue patterns in HRCT image series have the advantage to reduce the risk of omission of important lesions and provide a three-dimensional map of the categorized lung tissue to serve as a second opinion to the radiologist. Whereas automatic detection and quantification of the lung tissue patterns showed promising results in several studies,³⁻⁵ its aid for the clinicians is limited to

Further author information: (Send correspondence to Adrien Depeursinge, adrien.depeursinge@hevs.ch)

the challenge of image interpretation, letting the radiologists down with the problem of the final histological diagnosis. Complementary to lung tissue categorization, providing visually similar cases using content-based image retrieval (CBIR) is in accordance with the clinical workflow of the radiologists. CBIR of HRCT of the chest provides valuable information from cases with confirmed diagnoses and corresponds to the approach of the clinician with little experience who compares the image under investigation with typical cases listed in textbooks or contained in personal collections.^{6,7} CBIR of chest CT has rarely been proposed in the literature and the existing studies^{8–11} have presented systems for retrieving similar lung tissue types, which are of limited use in clinical practice. Moreover, all proposed systems require delineating query regions, which does not allow global inter-case similarity assessment including information from the whole lung. Retrieving similar cases in terms of histological diagnoses is closer to the needs of radiologists. The latter is however more challenging to implement as the content of the HRCT scans need to be analyzed as a whole. Each histological diagnosis of ILD is characterized by proportions and predominance of a given set of abnormal lung tissue patterns. In a previous study,¹² 3D case-based retrieval was introduced and evaluated based on the histological diagnoses. The inter-case distance was based on the differences of percentages of five lung tissue patterns within the whole lung, along with selected clinical parameters. The retrieval performances obtained suggest the feasibility of retrieving similar cases in terms of final histological diagnosis using CBIR. However, although known as being very discriminative for the differential diagnosis of ILDs,¹³ the localization of the diseased tissue was discarded by this approach. The goal of the work described in this article is to evaluate the benefits from using localized features for content-based image retrieval of HRCT images of the lung with ILDs. The retrieval performance is compared with the previous approach using the volume percent ages of five types of lung tissue as visual attributes without localization.¹²

1.1. Histological diagnoses and associated abnormal tissue locations

To identify the key locations of tissue disorders associated with ILDs, the most important lung tissue patterns and their corresponding localizations are detailed in Table 1 for seven frequent ILDs.¹³ As observed in Table 1, ground glass patterns are encountered in most of the ILDs and are thus non-specific. Therefore, its location as well as the clinical context and other HRCT findings are required to interpret the presence of ground glass.

- *Pulmonary fibrosis* (PF) means scarring throughout the lungs. The term fibrosis is used in this work to describe HRCT findings that are associated with the histological diagnosis PF and includes reticulation, traction bronchiectasis, architecture distortion and honeycombing. The characteristic basal and peripheral predominance of the abnormalities on HRCT scans is an important clue to the diagnosis of PF.¹⁴ Among the most common appearance reported in¹³ is lower lung zone with posterior predominance.
- *Tuberculosis* (TB) is an infectious disease caused by the inhalation of air-borne organisms (bacterias). Typically, the upper lobes are most affected. In patients with active TB signs include focal consolidation and cavitation.¹³ In miliary TB, a fine nodular pattern shows random distribution within the lung.¹³
- *Pneumocystis pneumonia* or *Pneumocystis carinii pneumonia* (PCP) is an opportunistic fungal infection, most common in human immunodeficiency virus (HIV) infected patients. Findings include patchy/diffuse ground glass, crazy-paving, cysts, pneumothorax and a central, perihilar or upper lobe distribution.
- *Hypersensitivity pneumonitis* (HP) is an allergic lung disease caused by breathing in a foreign substance. HRCT findings show patchy distribution of fibrosis, ground glass opacities or centri-lobular nodules.
- *Acute interstitial pneumonia* (AIP) is a disease causing rapid onset of respiratory failure. HRCT findings consist of patchy bilateral areas of ground glass opacities and diffuse or patchy consolidation.¹³
- *Cryptogenic organizing pneumonia* (COP), also known as Bronchiolitis obliterans organizing pneumonia, is a inflammatory process with presence of “granulation tissue polyps within the respiratory bronchioles and alveolar duct”.¹³ HRCT scans of the lung reveal patchy air-space consolidation, ground glass opacities, small nodular opacities, as well as bronchial wall thickening and dilation. These patchy opacities occur more frequently in the periphery of the lung and are often in the lower lung zone.¹⁵

Table 1. 7 common histological diagnoses of ILDs and associated HRCT findings according to.¹³

histological diagnosis	HRCT lung tissue patterns	predominance
Pulmonary fibrosis (PF)	fibrosis, bronchiectasis, ground glass	peripheral, sub-pleural, basal, posterior
Tuberculosis (TB)	micronodules (miliary), tree-in-bud, consolidation	diffuse, apical (cavitary)
Pneumocystis pneumonia (PCP)	ground glass, crazy-paving, cysts, pneumothorax	central, perihilar
Hypersensitivity pneumonitis (HP)	ground glass, emphysema, fibrosis	diffuse
Acute interstitial pneumonia (AIP)	ground glass, consolidation	basal, diffuse
Cryptogenic organizing pneumonia (COP ^a) ^a Bronchiolitis obliterans organizing pneumonia was formerly used and replaced by COP	ground glass, consolidation (patchy), macronodules, bronchial wall thickening, crazy-paving	peripheral, basal, peribronchovascular, subpleural
Sarcoidosis (SA)	micronodules, consolidation, macronodules, ground glass, fibrosis (end-stage)	apical, peribronchovascular, subpleural, peripheral

- *Sarcoidosis* (SA) is a systemic disorder of unknown origin. It is characterised by non-caseating granulomas that may resolve spontaneously or progress to fibrosis.¹³ The most characteristic findings are small nodules in a perilymphatic distribution. Common HRCT findings for SA are upper lobes and peribronchovascular predominance of confluent nodules or masses and fibrotic tissue in patients with end-stage disease.

1.2. Atlas-based localization of the features in CBIR

Localization is important for CBIR as the similarity between two images perceived by human observers strongly depends on the layout of the image as well as the spatial relations among depicted objects.¹⁶ Several approaches were proposed for localizing features for CBIR:¹⁷

- partitioning, which consists in extracting features at regularly sampled points,¹⁸
- salient points, where features are extracted at locations found by detectors (e.g. high-gradient, corner),¹⁶
- weak segmentation, features are extracted for each locally homogeneous region,¹⁹
- strong segmentation (or atlas-based), dividing the image into real world objects with prior knowledge.

In the context of content-based medical image retrieval, the variations among patients in terms of organ size, shape and location renders the localization tasks even more challenging. Moreover, similarity of medical images is often defined based on the type and extent of the disease as well as age and gender of the patient. The localizations of the features must be in accordance with the targeted diseases and the anatomy of the diseased organ. The use of regularly or randomly sampled points is hardly applicable to texture retrieval of the lung parenchyma as comparing lung tissue at locations that are not determined by the lung anatomy does not make

sense. The use of keypoint detectors is not adapted for texture analysis as the detectors are based on shape properties by placing salient points on edges or regions with high gradient values,¹⁶ whereas few detectors are based on texture properties.²⁰

The use of atlases including anatomical knowledge for feature localization is in accordance with the approach of radiologists with image interpretation. Moreover, ILDs have clearly defined predominances of appearance of the diseased lung tissue that are typical to each histological diagnosis (see Table 1), which suggests that an atlas-based localization of the features is appropriate. In,²¹ low-level features (e.g. shape, size, texture) are extracted in automatically segmented objects of interest for image retrieval. The objects are learned in a preliminary step. The system can then be tailored to a specific application (e.g. retrieval of brain lesions in magnetic resonance imaging (MRI) images). No quantitative evaluation of the system is carried out and the success of the proposed approach strongly depends on the segmentation performance, related to the complexity of the sought objects and thus to the medical application.

Concepts of using an indexed atlas to localize lesions for further CBIR of mammograms are detailed in.²² However the selection of the locations of the lesions within the atlas are manual, which does not enable automatic indexation of large image collections. In,²³ atlas-based localizations of the endoscope in upper digestive endoscopy is used for similar case retrieval. However, the retrieval is not based on the numerical content of images but on standardized descriptions of the studied case carried out by the physician.

Another imaging modality where atlas based localization is required is Positron emission tomography (PET). CBIR of brain PET images is not possible without using feature localization as most information is contained in the anatomic location of the activated region. CBIR of multi-dimensional dynamic PET images (3D and time) of the brain is investigated in.²⁴ The localization of volumes of interests within a standardized 3D anatomical atlas²⁵ is used as an additional feature for retrieval. Unfortunately, neither quantitative analysis of the retrieval performance nor systematic evaluation of the importance of the localization feature is carried out. In another study,²⁶ CBIR of neurological PET images based on Gabor wavelets and mean activity levels of specific anatomical regions is carried out. Again, no quantitative analysis of the retrieval performance is carried out.

1.2.1. Local features for CBIR of HRCT images of the chest

Atlas-based indexation of chest CTs has been little investigated. In,²⁷ similarity searching for chest CT images based on object features and spatial relation maps. In a first step, the lung lobes and the mediastinum are segmented using a tailored watershed algorithm. Then, shape-based features are extracted from the mediastinum region and texture attributes for the lung parenchyma as well as spatial relationships between the lung lobes and the mediastinum. The system uses a Euclidean distance in the feature space without feature weighting, which does not allow evaluating the contribution of the localization features in the retrieval performance.

Local versus global characterization of HRCT images for CBIR is investigated in.⁹ The ASSERT (Automatic Search and Selection Engine with Retrieval Tools) system uses low-level features either from hand-drawn regions in axial slices or from the whole lung. The distance from the centroid of the marked region and the nearest lung boundary point is also used as an additional feature. The empirical evaluation shows that using localized features significantly improves performance over using only global features. This study however shows several limitations. The localization information is only provided by the location of the delineated region and thus does not enable a systematic regional comparison among cases. Due to the requirement of delineating regions, the system can not be fully automatic and requires significant amount of work for annotating regions in all image series. At last, the low-level features are averaged over the whole lung which cannot be relevant information for indexing. For instance, severely injured lungs containing equal proportions of emphysema and consolidated tissue may have identical averaged grey-level value over the whole lungs as perfectly healthy lungs.

CBIR based on localized 2D features was reported in.²⁸ However, CBIR based on texture features localized in a three-dimensional referential has rarely been attempted in the literature, and never to our knowledge on HRCT images of the chest, where the appearance of the diseased patterns is very important for establishing the diagnosis of ILDs.²⁹ In a preliminary study,¹² we used a Euclidean distance based on the percentages of automatically segmented volumes of five lung tissue types as inter-case distance for CBIR. The latter showed feasibility of retrieving similar histological diagnoses based on image content although no localization information was used for visual indexation. However, to retrieve and show similar images with pathology, appearing at a

particular lung position was not possible. In this work, a 3D referential based on lung anatomy is utilized to localize features used for CBIR. The hypothesis under investigation is to test whether a systematic regional comparison of the percentages of five lung tissue types enables to learn the typical anatomical distribution of the lung tissue disorders that are specific to each histological diagnosis as shown in Table 1.

2. MATERIAL AND METHODS

In this section, the methods used for both global and localized content-based retrieval of HRCT images series with similar histological diagnosis are detailed. In Section 2.1, the database of ILD cases is described. Then, the various CBIR steps are explained in the following sequential order:

1. semi-automatic segmentation of the lung regions (Section 2.2),
2. blockwise texture classification of the lung parenchyma to generate a 3D map of the lung tissue (Section 2.3),
3. generation of the lung atlas from the lung masks segmented by step 1 (Section 2.4),
4. inter-case distance being either global or local (Section 2.5).

The validation strategy for retrieval performance estimation is described in Section 2.6.

2.1. Dataset

The dataset used is part of a database of ILD cases containing HRCT images with a slice thickness of 1mm and annotated regions performed by two radiologists at the University Hospitals of Geneva (HUG).³⁰ HRCT image series of 85 patients are used to evaluate the performance of the proposed approach. The diagnoses of each case was confirmed either by pathology (biopsy, bronchoalveolar washing) or by a laboratory/specific test. Seven ILD diagnoses were selected as being frequent and having sufficient number of cases, with a minimum of 3 cases for COP and 30 cases for PF. The distributions of the 7 ILDs diagnoses as well as marked regions of interest (ROI) are very unbalanced and representative of the respective prevalences in the Geneva area. Distributions of the annotated regions and histological diagnoses can be deduced from Tables 4 and 6 respectively.

2.2. Semi-automatic segmentation of lungs

The segmentation of the lung regions is a prerequisite for both texture-based categorization of the lung tissue and the generation of the lung atlas. Segmentation errors in the lung regions influence all further steps and a high accuracy is required. Since the geometries and shapes of the lungs are subject to large variations among cases due to various morphologies and extents of the disease, semi-automatic segmentation based on 3D region growing and 3D mathematical morphology is carried out with a graphical user interface (see Figure 2). 3D region growing mimics the propagation of air in lung volumes. The region growing routine is contained in YaDiV*. Starting from a seed point $s(x_s, y_s, z_s)$ defined by the user, each 26-connected neighbor is added to the region M_{lung} if the summed value of its own neighbors differs by less than a given variance v . M_{lung} describes the global lung regions well but contains many holes where the region growing algorithm was stopped by denser regions such as vessels or consolidations of the lung parenchyma. To fill these holes, a closing operation is applied to M_{lung} using a spherical structuring element. Two parameters require attention from the user: the radius r of the structuring element in millimeters and N_{op} which defines the number of closing operations.

*YaDiV: Yet Another Dicom Viewer, http://www.welfenlab.de/en/research/fields_of_research/yadiv/

2.3. 3D map of categorized lung tissue

The approach for categorizing lung tissue patterns associated with ILDs in HRCT relies on texture analysis. Four types of lung tissue disorders (i.e. emphysema, ground glass, fibrosis and micronodules) as well as healthy tissue are most common to the seven ILD diagnoses chosen. Features based on a grey-level histogram in Hounsfield Units (HU) are used. CT scanners deliver DICOM (Digital Imaging and COmunications in Medicine) images with pixel values in HU that can be univoquely mapped to the density of the observed tissue. Thus, essential information is contained directly in the grey-levels. To encode this information, 22 histogram bins bin_j of grey-levels in $[-1050; 600]$ corresponding to the interval of the lung HU values (including pathological) are used as texture features. An additional feature pix_{air} counts the number of air pixels which have value below -1000 HU. All lung tissue patterns depict nonfigurative and cellularly organized areas of pixels and have specific texture signatures. To describe texture properties, statistical measures from a tailored wavelet transform are extracted. Multiscale analysis using wavelet transforms proved to be adequate for texture analysis³¹ but requires to control the three essential affine parameters: translation, scale-progression and directionality. For lung tissue analysis, it is assumed that lung tissues patterns in transversal slices are translation and rotation-invariant, and isotropic mother wavelet functions are used. Moreover, a fine and initializable scale-progression is necessary to distinguish between vessels and micronodules. The quincunx scale-progression is finer than the widely used dyadic one with a subsampling factor of $\sqrt{2}$ instead of 2 and is used to oversample the wavelet filters in an overcomplete frame transform, which provides translation invariance. Additional justifications for using the described wavelet transform for lung tissue categorization can be found in.³²

Based on the lung mask M_{lung} , the lung parenchyma is analyzed in overlapping 32×32 blocks in 2D axial slices. The distance between the center of contiguous blocks is set to 4 pixels, which leads to a granularity of the analysis of 4×4 . For each block, the 22 histogram bins and the number of air pixels pix_{air} are concatenated into one hybrid feature vector \mathbf{v} along with parameters of Gaussian mixture models for each 8 iterations of the quincunx wavelet frame transform. A support vector machine (SVM) classifier is used to draw boundaries among the distinct classes of lung tissue represented in the feature space and to assign each block to one of the five lung tissue types. This step outputs a 3D map of the categorized lung tissue which can be used as a basis for both global and local-based similar case retrieval.

2.4. 3D anatomical atlas of the lungs

An anatomical atlas of the lung is used as a 3D referential to localize the various lung tissue types. The locations are chosen according to³³ and aim at distinguishing the predominant regions of the 7 ILDs as detailed in Table 1. The lungs are split perpendicularly to 4 axes. Vertically the lungs are divided into upper lung or apical, middle lung and lower lung or basal lung. The lungs are divided into anterior and posterior regions based on the intersection of the coronal and sagittal plane. The axial division results into central lung, intermediate and peripheral lung region. The regions are depicted in Figure 2. A finer localization of the lung tissue types is obtained using the intersection of all 10 regions, generating 36 sub-regions as depicted in Figure 1 (b) and (c). The patient orientations are aligned using the “image orientation” DICOM tag (0020,0037). Peribronchovascular locations, despite being relevant for several ILDs are not used as these would need more complex segmentation of the bronchial tree,³⁴ which is not conceivable with the high inter-slice gap imposed in the HRCT protocol. The next paragraphs describe the rules used to split the lungs perpendicularly to the four axes.

⊥ coronal and sagittal The center of mass $c_0(x_0, y_0, z_0)$ of M_{lung} is used as reference point to split the lungs. The left and right regions are defined as being all points of M_{lung} with $x \leq x_0$ and $x > x_0$ respectively. Similarly, the anterior and posterior regions are defined as being all points of M_{lung} with $y \leq y_0$ and $y > y_0$.

⊥ vertical The apical, central and basal regions are defined as $z < z_{max}/3$, $z_{max}/3 \leq z \leq 2z_{max}/3$ and $z > 2z_{max}/3$ respectively.

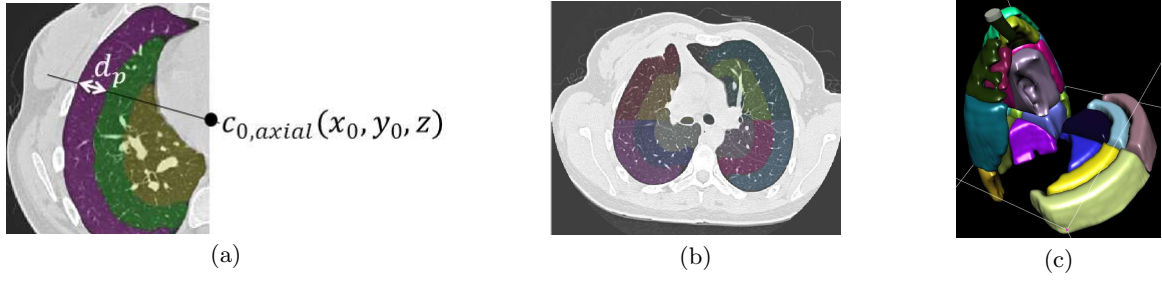


Figure 1. (a): definition of the peripheral region. (b) and (c): the 36 sub-regions resulting from the intersections of the 10 initial regions are used as the 3D localization system.

⊥ **axial** The division of M_{lung} into peripheral, middle and central regions is performed as follows:

1. the projection of c_0 is reported in each axial slice as $c_{0,axial}(x_0, y_0, z)$,
2. peripheral region is defined as all points of M_{lung} that are between a lung boundary and $c_{0,axial}$, and that are less distant from the lung boundary than a distance d_p (see Figure 1 (a)). d_p is arbitrarily chosen as the width of one single lung divided by 5.5 at a c_0 level to have approximately same widths for the three axial sub-regions,
 - (a) a 3D closing operation is applied using a spherical structural element with a radius of 5mm.
3. step 2 is repeated to the remaining voxels of M_{lung} to obtain the middle region,
4. the remaining voxels of M_{lung} are constituting the central region.

2.5. Global and local inter-case distances

Both inter-case distance measures are based on the percentages of each of the five lung tissue types. The global distance d_{global} is defined as the l_2 -Euclidean distance in the space of the differences δ of percentages of the tissue types:

$$d_{global} = \sqrt{\delta_h^2 + \delta_e^2 + \delta_g^2 + \delta_f^2 + \delta_m^2}, \quad (1)$$

where h stands for healthy, e for emphysema, g for ground glass, f for fibrosis and m for micronodules.

The inter-case distance is obtained by pairwise comparison of tissue distributions for the 36 sub-regions r :

$$d_{local} = \sum_{r=1}^{36} w_r \sqrt{\delta_{h_r}^2 + \delta_{e_r}^2 + \delta_{g_r}^2 + \delta_{f_r}^2 + \delta_{m_r}^2}, \quad (2)$$

where w_r are weights of each sub-region.


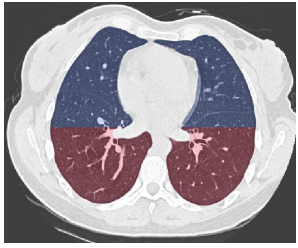
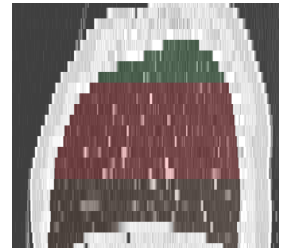
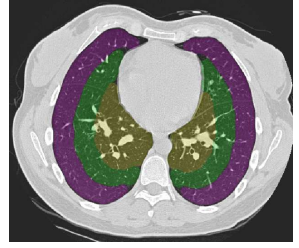
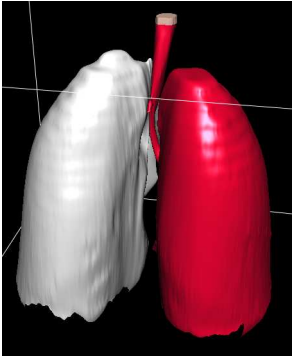
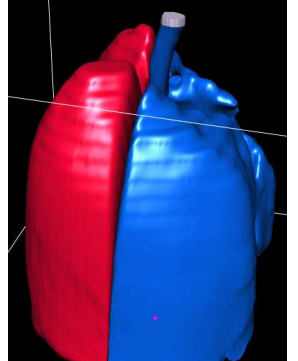
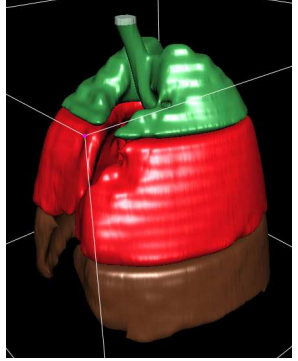
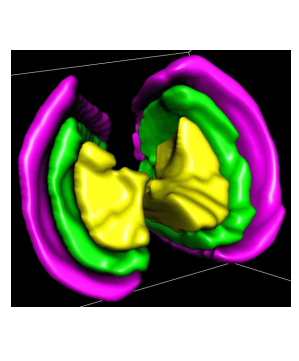
2.5.1. Optimization of the regional weights for the local inter-case distance

Obviously, not all anatomical locations are relevant for the characterization of the histological diagnoses. In order to promote the most important regions, the weights w_r in (2) are optimized using an exhaustive grid search in $[0 : 50]$ per axis. Due to computational constraints, a global grid search requiring to run the whole experiment 36^{50} times is not conceivable. Thus, the optimization is carried out per axis, where the regions are compared between each other per axis. For instance, in the vertical axis the retrieval performance is evaluated for each combination of three weights:

$$d_{local} = w_{apical}d_{apical} + w_{central}d_{central} + w_{basal}d_{basal}. \quad (3)$$

After obtaining optimal weights for each of the ten regions, the weight assigned to each of the 36 sub-regions is computed as the sum of normalized weights of each region from which it belongs. For instance, the region `apical_peripheral_anterior_left` obtains the weight $w = \tilde{w}_{apical_{best}} + \tilde{w}_{peripheral_{best}} + \tilde{w}_{anterior_{best}} + \tilde{w}_{left_{best}}$, where (\sim) denotes the per-axis normalization.

Table 2. Localization of the lung masks. The lung is split perpendicularly to 4 axes.

\perp coronal	\perp sagittal	\perp vertical	\perp axial
left, right	anterior, posterior	apical, central, basal	peripheral, middle, central
			
			

2.6. Experimental setup

The validation scheme for evaluating the retrieval performance is described in this section. In order to mimic a clinical use of the retrieval system, a leave-one-patient-out (LOPO) cross-validation (CV) is used, which enables assessing the retrieval performance obtained with a query case which is completely unknown from the system. The LOPO CV scheme is used to evaluate both lung tissue categorization and retrieval performance. For each query case, the lung tissue is fully classified using a classifier trained with all remaining cases. Then, the retrieval system returns the most similar cases based on either (1) or (2) from the remaining 84 cases.

3. RESULTS

The results obtained with each step of the retrieval system are presented in this section. Interpretations of the results and associated discussions can be found in Section 4.

3.1. Lung tissue categorization

The correctness of the lung tissue categorization is verified on a voxel-basis using the ground truth provided by the radiologists. The confusion matrix of the various tissue types is detailed in Table 3 and the associated classification performance in Table 4. An example of the lung tissue categorization is shown in Figure 2 (b).

3.2. Lung regions and 3D atlas

An example of the semi-automatic segmentation of the lung regions is depicted in Figure 2 (a). Our experience with the segmentation of 85 lung volumes is that the 3D region growing associated with closing allows an almost fully-automatic segmentation. The average time required to obtain a satisfactory lung mask varied from 30 seconds to 10 minutes, with a mean time of 4 minutes, leading to a total time of 5 hours 30 minutes for obtaining

Table 3. Confusion matrix of the lung tissue categorization in % obtained with the LOPO CV.

	healthy	emphysema	ground glass	fibrosis	micronodules
healthy	79	7.8	6.5	7.3	5.9
emphysema	4.4	69.2	3.9	15.8	6.7
ground glass	9.4	1.7	59.3	22.9	6.7
fibrosis	4.6	3.4	9.2	80.5	2
micronodules	9.9	2.6	3.9	13.5	70.2

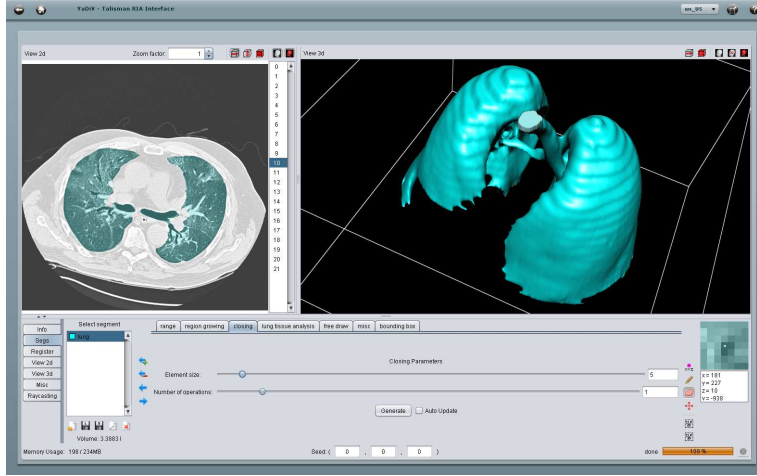
Table 4. Performance measures in % associated with Table 3. N_{vox} and N_{cases} denote the number of voxels and cases used for evaluation. Global geometric and arithmetic mean accuracies of 88.5% and 71.6% are achieved respectively.

	recall	precision	F-measure	accuracy	N_{vox}	N_{cases}
healthy	79	49.6	61	90.7	441'472	5
emphysema	69.2	49.7	57.8	95.7	204'536	5
ground glass	59.3	67.8	63.3	88.3	813'689	23
fibrosis	80.5	64.6	71.7	84.5	1'162'803	30
micronodules	70.2	92.8	79.9	84.1	2'157'766	14

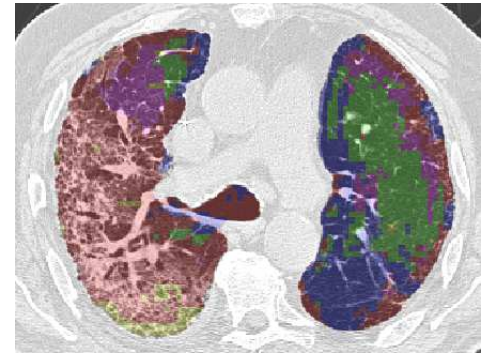
the 85 lung masks. Manual corrections are required when the closing operation cannot fill large regions of consolidated tissue. Given that the 3D region growing mimics the propagation of air in the lung volumes, the trachea is naturally included in M_{lung} .

3.3. Case-based retrieval

The optimal weights w_r obtained with the optimization strategy described in Section 2.5.1 using various targeted performance measures are shown in Table 5. The retrieval performance using d_{global} and d_{local} with weights favoring either mean P@1 or mean P@ N_r are detailed in Table 6. The performance obtained using a global Euclidean distance with each percentages of lung tissue type in each region (36×5 dimensions) were lower than



(a)



(b)

Figure 2. (a): segmentation of the lung volumes using YaDiV. A closing tab was added to YaDiV to perform a closing operation after the region growing. (b): an example of the color-coded lung tissue categorization. Colors are attributed as follows: green for healthy, blue for emphysema, yellow for ground glass, red for fibrosis and pink for micronodules.

Table 5. Weights w_r obtained with the optimization strategy described in Section 2.5.1. Numbers in bold are where a medical signification was found (more details in Section 4.3). The weights obtained when targeting performance measures of PCP, AIP and COP are not shown as being in most cases equal to 0 as discussed.

histological diagnosis	targeted performance	vertical			axial			sagittal		lateral	
		apical	central	basal	peripheral	middle	central	anterior	posterior	left	right
PF	P@1	0	1	4	1	0	1	7	4	2	3
	P@($N_r = 30$)	0	14	9	1	0	0	3	38	16	1
TB	P@1	0	1	0	0	0	1	0	1	0	1
	P@($N_r = 12$)	7	4	2	6	1	1	1	3	0	1
HP	P@1	0	3	2	0	1	1	4	1	1	0
	P@($N_r = 16$)	1	10	0	6	1	4	0	1	6	1
SA	P@1	10	9	6	0	3	4	1	0	1	3
	P@($N_r = 16$)	3	4	0	3	1	13	1	0	1	3
global mean (case-based)	P@1	0	4	15	3	0	4	5	1	12	19
	P@ N_r	8	11	25	16	0	1	41	3	11	13.5

Table 6. Retrieval performance with the LOPO CV for d_{global} and d_{local} using weights favoring either P@1 or P@ N_r . Bold numbers show best performance.

histological diagnosis	cases	d_{global} as defined in (1)				d_{local} as defined in (2), with weights favoring P@1				d_{local} as defined in (2), with weights favoring P@ N_r			
		P@1	P@5	P@10	P@ N_r	P@1	P@5	P@10	P@ N_r	P@1	P@5	P@10	P@ N_r
PF	30	50	50	48	40.9	63.3	39.3	35	31.7	56.7	42.7	35	35.7
TB	12	33.3	31.7	22.5	21.5	33.3	21.7	25	23.6	33.3	11.7	21.7	22.7
PCP	4	0	10	5	12.5	25	10	5	12.5	25	15	7.5	18.7
HP	16	43.7	26.2	21.9	21.1	37.5	20	19.4	20.3	25	22.5	20.6	21.1
AIP	4	0	0	0	0	0	0	2.5	0	0	0	2.5	0
COP	3	0	6.7	6.7	11.1	66.7	13.3	6.7	22.2	66.7	13.3	6.7	22.2
SA	16	31.2	28.7	25.6	24.6	62.5	43.7	39.4	31.6	56.2	38.7	38.1	31.2
mean (case-based)	85	36.5	33.2	29.5	27.1	49.4	29.8	27.5	25.7	43.5	29.4	27.2	27.3
mean (class-based)	85	24.4	23.3	19.9	19.8	42.2	22.2	20.1	21	38.3	21.7	19.9	22.4

the ones with the weighting scheme, which was also the case when using equivalent weight for each region (e.g. $w_r = 1 \forall r$ in Eq. (2)).

4. INTERPRETATION

The results presented in Section 3 were obtained with the various steps of the retrieval system described in Section 2 and are interpreted here.

4.1. Lung segmentation and 3D atlas

The trachea is included in M_{lung} in most cases, which may bias the volume percentages of the five patterns in Eq. (1) and (2). The trachea is classified either as emphysema because it contains air, or as fibrosis which also contains air bubbles and is a class favored by the SVM because it has a high number of instances. The construction of the 3D atlas from M_{lung} was in general successful, although no quantitative evaluation is carried out due to a lack of ground truth. Minor problems were observed with the separation of the left and right regions when the right and the left lung were naturally overlapping. A quality control was carried out, and although no pixelwise manual corrections were added, some regions (e.g. left/right, anterior/posterior and apical/central/basal) were inverted due to errors in the “image orientation” DICOM tag.

4.2. Lung tissue classification

The 5-class lung tissue classification reaches a geometric mean of 88.5%, which suggests that the 3D map of categorized lung tissue provides an appropriate estimation of both spatial and cardinal distribution of the diseases to be used for case-based retrieval. Ground glass has the weakest recall of 59.3, and is mixed 22.9 times over 100 with fibrosis. This recurrent mistake can be partly explained by the available ground truth: fibrosis patterns always contain a small percentage of ground glass, due to the redistribution of the perfusion which has been annotated as fibrosis and thus introduces noise in the training examples. Fibrosis and micronodules have a high number of false positives due to their dominant representation in the dataset as SVMs tends to favor large classes to maximize global accuracy. Some classification errors appear close to the lung boundary where wavelet coefficients from large scales are influenced by the lung borders.

4.3. Case-based retrieval

The optimal weights found for diagnoses PCP, AIP and COP are most often close to zero. The latter diagnoses are containing a small number of cases (4, 4 and 3 respectively), suggesting that not enough data is available to have a representative distribution of the abnormal tissue specific to these diagnoses. After analysis of the optimal weights obtained for the diagnoses in Table 5, justifications could be found for several observations that are consistent with prior medical knowledge detailed in Table 1 and in Section 1.1.

- *Pulmonary fibrosis* High weights obtained for central, basal, peripheral and posterior regions all are in accordance with medical knowledge. According to,¹³ idiopathic PF is known to have peripheral, basal and sub-pleural predominance in 70% of the cases. Honeycombing HRCT finding is also predominant in the lower lung and posterior zone.
- *Tuberculosis* Apical regions are promoted by the weighting scheme, which is in accordance with the fact that many cases of cavitary TB, pleural abnormalities represent the sequela of underlying parenchymal disease and are apical in location. In addition, micronodules that are characteristic to the miliary TB are easier to detect in the peripheral region due to smaller and less visible bronchovascular structures.
- *Sarcoidosis* Upper parts of the lungs are favored by the weighting scheme and is consistent with the expected distribution of micronodules with SA that is peribronchovascular in the central lung and upper lobes.

For all diagnoses, peripheral and basal regions are promoted by the system, which is indeed the siege of several histological diagnoses of ILDs. It can be observed in Table 6 that the weighting scheme enables to tune the system to favor a given disease at a given performance measure.

When compared to global inter-case distance d_{global} , region-based retrieval using d_{local} clearly improves early precision (P@1) as it can be observed in Table 6. Localized comparisons of the tissue percentages with d_{local} have not the same effect on all diagnoses. It is obvious that d_{local} globally improves retrieval performance for diagnoses SA, PCP and COP. However, only early precision is improved for PF, whereas the d_{global} enables better retrieval when looking at the precision after $N > 3$ results. For HP, global-based retrieval performs better than local, which can be explained by the fact that the disease has a patchy but diffuse (non-localized) distribution within the lung. No clear trend can be deduced for TB. In order to benefit from both approaches, a fusion of d_{global} and d_{local} may help to use localization only for the diseases having a characteristic predominance. Beyond

improving the quantitative evaluation of the early retrieval performance, we believe that local retrieval improves the quality of the retrieved cases in terms of visual similarity.

It worth noting that no LOPO CV is used to choose the regional weights w_r , which may introduce a risk of overfitting the data and slightly bias the retrieval performance in Table 6. A risk of inducing false alarms to the radiologists is also present as no control cases are contained in the database and the retrieval system can only retrieve positive cases. When interpreting performances in Table 6, it is also important to keep in mind that the link between visual similarity of two HRCT scans and their associated diagnoses is not straightforward. Finally, a system showing cases that are visually similar but with distinct diagnoses prevents the reader from mixing diagnoses with similar radiological findings, which is difficult to assess with the quantitative evaluation.

5. CONCLUSIONS

The CBIR approach proposed in this work provides complementary information, from past cases with confirmed diagnoses, to lung tissue classification and quantification in HRCT. The system exploits the locations of the pathological lung tissue and allows significant improvement in terms of early retrieval precision when compared to the approach based on global features only. The distribution of the optimal regional weights is in accordance with medical knowledge. The weighting scheme allows to tune the system by optimizing the retrieval performance of a given diagnosis at a given performance measure (e.g. P@1, P@10). The limited performance observed for some of the diagnoses can partially be explained by the fact that the link between visual similarity of two HRCT scans and their associated diagnoses is not straightforward. The system provides an objective inter-case similarity measure enabling advanced browsing in large collections of cases.

Acknowledgments

This work was supported by the Swiss National Science Foundation (FNS) with grants 200020-118638 and 205321-130046 as well as the EU 7th Framework Program in the context of the Khresmoi project (FP7-257528).

REFERENCES

1. T. E. King, *Approach to the adult with interstitial lung disease: clinical evaluation*, UpToDate, Waltham, MA, Denise S. Basow ed., 2010.
2. G. W. Hunninghake, D. A. Lynch, J. R. Galvin, B. H. Gross, N. Müller, D. A. Schwartz, T. E. King, J. P. Lynch, R. Hegele, J. Waldron, T. V. Colby, and J. C. Hogg, “Radiologic Findings Are Strongly Associated With a Pathologic Diagnosis of Usual Interstitial Pneumonia,” *Chest* **124**(4), pp. 1215–1223, 2003.
3. Y. Uchiyama, S. Katsuragawa, H. Abe, J. Shiraishi, F. Li, Q. Li, C.-T. Zhang, K. Suzuki, and K. Doi, “Quantitative computerized analysis of diffuse lung disease in high-resolution computed tomography,” *Medical Physics* **30**, pp. 2440–2454, September 2003.
4. E. A. Hoffman, J. M. Reinhardt, M. Sonka, B. A. Simon, J. Guo, O. Saba, D. Chon, S. Samrah, H. Shikata, J. Tschirren, K. Palagyi, K. C. Beck, and G. McLennan, “Characterization of the interstitial lung disease via density-based and texture-based analysis of computed tomography images of lung structure and function,” *Academic Radiology* **10**, pp. 1104–1118, October 2003.
5. I. C. Sluimer, P. F. van Waes, M. A. Viergever, and B. van Ginneken, “Computer-aided diagnosis in high resolution CT of the lungs,” *Medical Physics* **30**, pp. 3081–3090, December 2003.
6. C. Brodley, A. Kak, C. Shyu, J. Dy, L. Broderick, and A. M. Aisen, “Content-based retrieval from medical image databases: A synergy of human interaction, machine learning and computer vision,” in *Proceedings of the 10th National Conference on Artificial Intelligence*, pp. 760–767, (Orlando, FL, USA), July 1999.
7. A. M. Aisen, L. S. Broderick, H. Winer-Muram, C. E. Brodley, A. C. Kak, C. Pavlopoulou, J. Dy, C.-R. Shyu, and A. Marchiori, “Automated storage and retrieval of thin-section CT images to assist diagnosis: System description and preliminary assessment,” *Radiology* **228**, pp. 265–270, July 2003.
8. C.-R. Shyu, C. E. Brodley, A. C. Kak, A. Kosaka, A. M. Aisen, and L. S. Broderick, “ASSERT: A physician-in-the-loop content-based retrieval system for HRCT image databases,” *Computer Vision and Image Understanding* **75**(1/2), pp. 111–132, 1999.

9. C. R. Shyu, C. E. Brodley, A. C. Kak, A. Kosaka, A. Aisen, and L. Broderick, "Local versus global features for content-based image retrieval," in *Content-Based Access of Image and Video Libraries, 1998. Proceedings. IEEE Workshop on*, pp. 30–34, June 1998.
10. C.-T. Liu, P.-L. Tai, A. Y.-J. Chen, C.-H. Peng, and J.-S. Wang, "A content-based medical teaching file assistant for CT lung image retrieval," in *Proceedings of the IEEE International Conference on Electronics, Circuits, Systems (ICECS2000)*, pp. 361–365, (Jouneih-Kaslik, Lebanon), December 2000.
11. Y. Tao, X. S. Zhou, J. Bi, A. Jerebkoa, M. Wolf, M. Salganicoff, and A. Krishnana, "An adaptive knowledge-driven medical image search engine for interactive diffuse parenchymal lung disease quantification," *Medical Imaging 2009: Computer-Aided Diagnosis* **7260**(1), p. 726007, SPIE, 2009.
12. A. Depeursinge, A. Vargas, A. Platon, A. Geissbuhler, P.-A. Poletti, and H. Müller, "3D case-based retrieval for interstitial lung diseases," in *MCBR-CDS 2009: Medical Content-based Retrieval for Clinical Decision Support*, B. Caputo, H. Müller, T. Syeda-Mahmood, J. Kalpathy-Cramer, and J. Duncan, eds., *Lecture Notes in Computer Science (LNCS)*, pp. 39–48, Springer, February 2010.
13. W. R. Webb, N. L. Müller, and D. P. Naidich, eds., *High-Resolution CT of the Lung*, Lippincott Williams & Wilkins, Philadelphia, USA, 2001.
14. C. A. Souza, N. L. Müller, J. Flint, J. L. Wright, and A. Churg, "Idiopathic pulmonary fibrosis: Spectrum of high-resolution CT findings," *American Journal of Roentgenology* **185**, pp. 1531–1539, December 2005.
15. M. Ujita, E. A. Renzoni, S. Veeraraghavan, A. U. Wells, and D. M. Hansell, "Organizing Pneumonia: Perilobular Pattern at Thin-Section CT," *Radiology* **232**(3), pp. 757–761, 2004.
16. D. G. Lowe, "Distinctive image features from scale-invariant keypoints," *International Journal of Computer Vision* **60**(2), pp. 91–110, 2004.
17. H. Müller, *User Interaction and Performance Evaluation in Content-Based Visual Information Retrieval*. PhD thesis, Computer Vision and Multimedia Laboratory, University of Geneva, Geneva, Switzerland, June 2002.
18. T. Westerveld, "Image retrieval: Content versus context," in *Recherche d'Informations Assistée par Ordinateur (RIA'O'2000) Computer-Assisted Information Retrieval*, **1**, pp. 276–284, CID, (Paris, France), April 2000.
19. A. Winter and C. Nastar, "Differential feature distribution maps for image segmentation and region queries in image databases," in *IEEE Workshop on Content-based Access of Image and Video Libraries (CBAIVL'99)*, pp. 9–17, (Fort Collins, Colorado, USA), 22 1999.
20. J. Zhang, M. Marszalek, S. Lazebnik, and C. Schmid, "Local features and kernels for classification of texture and object categories: A comprehensive study," in *Computer Vision and Pattern Recognition Workshop, 2006. CVPRW '06. Conference on*, p. 13, June 2006.
21. W. W. Chu, C.-C. Hsu, A. F. Cárdenas, and R. K. Taira, "Knowledge-based image retrieval with spatial and temporal constructs," *IEEE Transactions on Knowledge and Data Engineering* **10**(6), pp. 872–888, 1998.
22. H. Alto, R. Rangayyan, R. Paranjape, J. Desautels, and H. Bryant, "An indexed atlas of digital mammograms for computer-aided diagnosis of breast cancer," *Annals of Telecommunications* **58**, pp. 820–835, 2003.
23. C. Le Guillou, J. M. Cauvin, B. Solaiman, M. Robaszkiewicz, and C. Roux, "Knowledge representation and cases indexing in upper digestive endoscopy," in *Engineering in Medicine and Biology Society, 2000. Proceedings of the 22nd Annual International Conference of the IEEE*, **1**, pp. 9–12, July 2000.
24. H. Wu, J. Kim, W. Cai, and D. D. Feng, "Volume of interest (VOI) feature representation and retrieval of multi-dimensional dynamic positron emission tomography images," in *Intelligent Multimedia, Video and Speech Processing, 2004. Proceedings of 2004 International Symposium on*, pp. 639–642, October 2004.
25. S. Minoshima, R. A. Koeppe, K. A. Frey, and D. E. Kuhl, "Anatomic Standardization: Linear Scaling and Nonlinear Warping of Functional Brain Images," *Journal of Nuclear Medicine* **35**(9), pp. 1528–1537, 1994.
26. S. Batty, J. Clark, T. Fryer, and X. Gao, "Prototype system for semantic retrieval of neurological PET images," in *Medical Imaging and Informatics*, X. Gao, H. Müller, M. Looms, R. Comley, and S. Luo, eds., *Lecture Notes in Computer Science* **4987**, pp. 179–188, Springer Berlin / Heidelberg, 2008.

27. S.-N. Yu and C.-T. Chiang, "Similarity searching for chest CT images based on object features and spatial relation maps," in *Engineering in Medicine and Biology Society, 2004. EMBS '04. 26th Annual International Conference of the IEEE*, **1**, pp. 1298–1301, September 2004.
28. T. Zrimec and I. Lajovic, "A medical image assistant for efficient access to medical images and patient data," *The Journal on Information Technology in Healthcare* **7**, pp. 261–271, October 2009.
29. T. Zrimec and J. S. J. Wong, "Improving computer aided disease detection using knowledge of disease appearance," in *MEDINFO 2007. Proceedings of the 12th World Congress on Health (Medical) Informatics, Studies in Health Technology and Informatics* **129**, pp. 1324–1328, IOS Press, August 2007.
30. A. Depeursinge, A. Vargas, A. Platon, A. Geissbuhler, P.-A. Poletti, and H. Müller, "Building a reference multimedia database for interstitial lung diseases," *Computerized Medical Imaging and Graphics*, submitted.
31. M. Unser, "Texture classification and segmentation using wavelet frames," *IEEE Transactions on Image Processing* **4**, pp. 1549–1560, November 1995.
32. A. Depeursinge, D. Van De Ville, A. Platon, A. Geissbuhler, P.-A. Poletti, and H. Müller, "Affine-invariant texture learning for the characterization of lung tissue in HRCT using isotropic wavelet frames," *IEEE Transactions in Medical Imaging*, submitted.
33. T. Zrimec, S. Busayarat, and P. Wilson, "A 3D model of the human lung," in *Proceedings of MICCAI 2004*, S. LNCS, ed., **3217**, pp. 1074–1075, October 2004.
34. D. Aykac, E. A. Hoffman, G. McLennan, and J. M. Reinhardt, "Segmentation and analysis of the human airway tree from three-dimensional X-ray CT images," *IEEE Transactions on Medical Imaging* **22**, pp. 940–950, August 2003.